Microsc. Microanal. 9, 574–580, 2003
DOI: 10.1017/S1431927603030277

Microscopy AND Microanalysis

Analysis of Orientations of Collagen Fibers by Novel Fiber-Tracking Software

Jun Wu,[1] Bartłomiej Rajwa,[2,3] David L. Filmer,[1] Christoph M. Hoffmann,[4] Bo Yuan,[4] Ching-Shoei Chiang,[4] Jennie Sturgis,[2] and J. Paul Robinson[2,5]*

[1]*Department of Biology, Purdue University, West Lafayette, IN 47907, USA*
[2]*Department of Basic Medical Sciences, Purdue University, West Lafayette, IN 47907, USA*
[3]*Department of Biophysics, The Jan Zurzycki Institute of Molecular Biology and Biotechnology, Jagiellonian University, ul. Gronostajowa 7, 30-387 Kraków, Poland*
[4]*Department of Computer Science, Purdue University, West Lafayette, IN 47907, USA*
[5]*Department of Biomedical Engineering, Purdue University, West Lafayette, IN 47907, USA*

Abstract: Recent evidence supports the notion that biological functions of extracellular matrix (ECM) are highly correlated to not only its composition but also its structure. This article integrates confocal microscopy imaging and image-processing techniques to analyze the microstructural properties of ECM. This report describes a two- and three-dimensional fiber middle-line tracing algorithm that may be used to quantify collagen fibril organization. We utilized computer simulation and statistical analysis to validate the developed algorithm. These algorithms were applied to confocal images of collagen gels made with reconstituted bovine collagen type I, to demonstrate the computation of orientations of individual fibers.

Key words: image processing, confocal microscopy, ECM, collagen fibers, orientation

Introduction

In tissues, cells reside within extracellular matrix (ECM)—an organized three-dimensional network composed of collagens, elastin, glycoproteins, proteoglycans (PGs), and glycosaminoglycans (GAGs), which they secrete and mold into the intercellular space. These molecules are synthesized by chondrocytes, osteocytes, fibroblasts, epithelial cells, and other specialized cells. ECM exerts control over cells and the reciprocal communication between cells and plays an important role in modulation of critical physiologic and pathologic processes, including proliferation, survival, migration, and differentiation (Kleinman et al., 1981; Bissell et al., 1982; Yamada, 1983; Adams & Fiona, 1993; Aumailley & Gayraud, 1998).

It has been demonstrated that geometrical or topological considerations also contribute to modulation of cell responses to environment, and many aspects of ECM signaling indeed depend on its function as a mechanical component (Berthiaume et al., 1996; Chen et al., 1997; Curtis & Wilkinson, 1998). The degree of cell spreading is controlled by the three-dimensional architecture of ECM (Chen et al., 1997; Choquet et al., 1997; Pelham & Wang, 1997; Stepien et al., 1999). In this way ECM can orchestrate cell locomotion, anchorage-dependent cell growth, suppression of apoptosis, and modulation of gene expression (Lo et al., 2000; Wang et al., 2000).

It is known that the dominant structural components of ECM are collagens (Aumailley & Gayraud, 1998). This

Received September 19, 2002; accepted December 10, 2002.
*Corresponding author. E-mail: jpr@flowcyt.cyto.purdue.edu

has generated a considerable interest in determining collagen fiber length, orientation, and diameter in nonprocessed and nonfixed collagen matrices (Brightman et al., 2000; Ottani et al., 2001; Voytik-Harbin et al., 2001; Roeder et al., 2002). However, the complexity, density, and thickness of those three-dimensional networks make observation, visualization, and extraction of quantitative information very difficult.

To quickly and accurately quantify collagen fiber organization, we developed middle-line tracing software.[1] The software is able to compute fiber orientation (also diameter and length; results not shown) on the basis of three-dimensional confocal data sets. Traditional tracking algorithms investigate the neighbors of each pixel on a single-pixel midline.

In this report we demonstrate an application of a new fiber-tracking algorithm, which is able to analyze confocal images and compute orientations of each individual fiber present in collagen matrices. We utilized our image-processing software to reveal orientational anisometry of gels formed from reconstituted type I collagen.

Methodology

Sample Preparation and Image Acquisition

Purified type I collagen from bovine dermis (Collagen Corporation, Fremont, CA) was obtained as a sterile solution in 0.012 N HCl. Eight milliliters of chilled collagen were mixed with 1 ml PBS. One milliliter of 0.1 M NaOH was added and mixed. The pH of the solution was adjusted to 7.4 ± 0.2 by the addition of a few drops of 0.1 M HCl or 0.1 M NaOH. Collagen gelation was initiated in Lab-Tek chambered cover glasses by warming the neutralized solution to 37°C.

Samples were imaged without staining using the Bio-Rad MRC1024 (Bio-Rad Laboratories, Hemel Hempstead, UK) confocal microscope via a 60×, 1.4-NA oil-immersion lens. Illumination was provided by a 488-nm laser and backscattered light was detected by a photomultiplier tube. *X-y* plane pixel size was set to 0.1–0.25 μm. A z-step of 0.2–0.6 μm was used to optically section the sample. Three-dimensional data sets consisted of 50 to 80 image slices. Image reconstruction was prepared using Image Pro Plus package (Media Cybernetics, Inc., Silver Spring, MD).

Computer Simulation and Nonparametric Statistical Analysis

To test our fiber-tracking software, we prepared artificial images simulating real confocal images of collagen. Digital images contained straight lines (straight cylinders) or sine waves (cylinder-connected sine waves). To simulate fiber by straight lines in a two-dimensional image, a pair of points was randomly selected, and then connected with a line of either predetermined or random width. Thus the simulated fiber had a random orientation and length. Alternatively, a standard sine wave was created with a random length, then rotated to a random orientation, and translated to a randomly selected point in the image. To simulate fibers in three-dimensional space, we created three-dimensional geometrical objects distributed in three-dimensional space with random length, orientation, and diameter. Finally, the three-dimensional space was converted to a set of images mimicking image slices collected by a confocal microscope.

Kuiper's test was used to describe our data statistically. Kuiper's test improves Kolmogorov–Smirnov statistics, adapting it to circular data such as the distribution of orientations. The validation of our tracing software was tested by comparing the distributions of computed data to distributions of actual data.

Tracking Algorithm

We applied our fiber-tracing software to (a) identify the midlines of fibers, (b) recognize and maintain cross-links (intercross) between fibers, and (c) calculate orientation of fibers. For all images, we first applied a Euclidean distance map (EDM) to encode the brightness of every pixel (voxel) on the image as the distance to the nearest pixel (voxel) in the background. A disk with regulated radius was used as a tracing element in two dimensions. To avoid substantial increases in algorithm complexity and computational time we selected a cube (instead of a sphere) to trace the fibers in three dimensions.

The critical step in the algorithm was choice of the initial tracing position. As shown in Figure 1, the tracing procedure starts from the global maximum distance point (GMDP; an unlabeled point in an image with the largest EDM mapping value, such as point *O*), finds local maximum distance points (LMDP; an unlabeled point with a

[1]The software is based on an algorithm that is in a Ph.D. thesis (Wu, 2002).

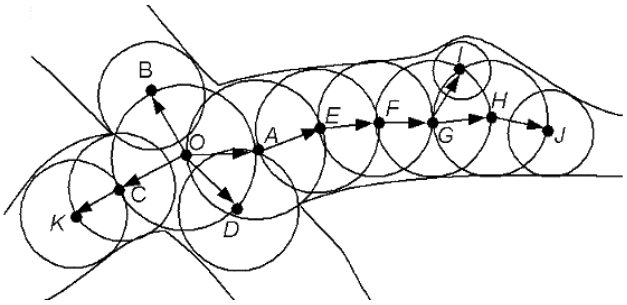

Figure 1. Fiber-tracking algorithm illustrated in two-dimensional space. Tracing procedure starts from GMDP (point *O*), finds LMDPs (points *A*, *B*, *C*, and *D*) on the perimeter of the circle, and then forms branches along midlines (*OA*, *OB*, *OC*, and *OD*). Following each branch (such as *OA*), the procedure repeats tracing from a new tracing center (such as point *A*), and adds the found LMDPs (*E*, *F*, and *G*) subsequently to the branch to extend it (such as branch *OAEFG*). The procedure then starts again from point *G* to create new branches following directions *GI* and *GH*. The procedure continues until the end of a fiber is reached and then starts from a new unlabeled GMDP to search other fibers.

larger EDM mapping value than its neighbors on the perimeter of the circle or the faces of the cube), such as points *A*, *B*, *C*, and *D*, and then forms branches along midlines (*OA*, *OB*, *OC*, and *OD*). Then, a disk (or a cube) with a center at point *O* and a radius (half the edge) equal to the mapped distance is labeled. The procedure follows one of the branches (such as *OA*), and repeats the tracing from a new tracing center (point *A*). In the next step, the procedure adds LMDPs (such as *E*, *F*, and *G*) that are found subsequently to the branch, extending it (such as branch *OAEFG*). The procedure then starts again from point *G* to create new branches following directions *GI* and *GH*. The procedure continues until the fiber end is reached and then starts from a new unlabeled GMDP to search for other fibers. The orientation of the branch is measured by linear regression of all the labeled points belonging to it. Unlike two-dimensional orientation, three-dimensional orientation is described by a pair of angles projected onto the *x*-*y* and *x*-*z* planes.

To identify the midline of a fiber it was necessary to remove the side branches like *GI*, which had only one free terminal (i.e., no connection to other branches) and a very short length. Following this some of the remaining branches were connected to form continuous midlines. If the terminal had only one connection, the branches were connected to form one midline segment, as *OAEFG* connects *GHJ* . . . to form *OAEFGHJ*. . . . If the terminal had multiple connections, the branches with similar orientations were connected. For example, *OCK* . . . connects *OAEFGHJ* . . . , while *OB* . . . connects *OD* . . . at terminal *O*. Thus, the cross-links at *O* were maintained, and each midline had two free terminals.

Results

Software Validation

Two types of synthetic images were used to evaluate the accuracy of quantitative data extracted by the algorithm: straight-line images and sine-wave images. Four groups of images were created. Group I consisted of three two-dimensional images; each image had 20 nonintersecting synthetic straight lines with lengths varying from 20 to 300 pixels. Group II consisted of six two-dimensional images, each of which had 20 sine waves with lengths varying from 50 to 100 pixels. Group III consisted of two three-dimensional image sets, each with 50 images. Here 40 straight lines were distributed in the image space with lengths varying from 20 to 260 pixels. Group IV consisted of four three-dimensional image sets with 100 images each. This group had a total of 85 sine waves distributed in three-dimensional space with lengths varying from 50 to 100 pixels.

Statistical analysis was used to evaluate differences between the computed data distribution and actual data distribution. The results of statistical analysis of two-dimensional and three-dimensional data are listed in Table 1, where N_1 and N_2 are the number of synthetic objects and the number of midlines extracted by the algorithm. The p values in both panels were greater than .05. The large p value indicated that there was no reason to reject the notion that the distribution of computed data came from the same distribution as that of the actual data, based on a significance level of .05. From these statistical analyses, a conclusion can be made that the distributions in both computed data and actual data are identical.

Testing of the Algorithm Accuracy

To test the algorithm accuracy in measuring fiber orientation in three-dimensional space, nine groups of data sets, each with 10 image sets, were created. Each image set consisted of 200 synthetic images (200 × 200 pixels), and

Table 1. The Kuiper's Test for Orientation Distributions of Computed and Actual Data in Two-Dimensional Synthetic Images (Panel a) and Three-Dimensional Synthetic Image Sets (Panel b).[a]

Panel a: Two-dimensional synthetic images

	Data size	Orientation distribution test
2D-lines	$N_1 = 60$	$K = 0.053279$
	$N_2 = 61$	$K_a = 0.293023$
		$p = 1.0000$
2D-curves	$N_1 = 120$	$K = 0.080992$
	$N_2 = 121$	$K_a = 0.628660$
		$p = 0.9996$

Panel b: Three-dimensional synthetic image sets

	Data size	*x-y* orientation distribution test	*x-z* orientation distribution test
3-D lines	$N_1 = 80$	$K = 0.082065$	$K = 0.220109$
	$N_2 = 92$	$K_a = 0.536826$	$K_a = 1.439832$
		$p = 1.0000$	$p = 0.2308$
3-D curves	$N_1 = 85$	$K = 0.128561$	$K = 0.178030$
	$N_2 = 83$	$K_a = 0.833113$	$K_a = 1.153683$
		$p = 0.9650$	$p = 0.6047$

[a]The N_1 and N_2 in the table are the number of synthetic objects and the number of midlines extracted by developed software.

had the same number of randomly generated cylinders. The number of generated fibers ranged from 4 to 36.

After processing by the developed algorithm, the computed orientation data were compared to simulated actual data to compute the error. For each computed orientation pair (*xy* angle and *xz* angle), the matched orientation pair in actual data was identified from which the squared error was computed. Finally, the mean square error of the orientation measurement in each image set was computed. Figure 2 depicts the mean and standard deviation of the computational error in measuring *xy* angle and *xz* angle for each group of image sets. The results show that mean errors of both *xy* angle and *xz* angle increased with the number of synthetic fibers, but were always smaller than 1.4°.

Quantification of Fiber Orientation in Three-Dimensional Collagen Matrix

After being tested by computer simulation and statistical analysis, the tracking software was applied to confocal images. Gels of bovine collagen type I were synthesized and imaged with a confocal microscope operating in backscattered–light mode as previously described. Figure 3 presents the three-dimensional view of a representative data set. The three-dimensional quantitative data describing fiber orientation were computed by the developed software. Figure 4 shows a representative plot of fiber orientations. The plot shows that most *xz* angles are clustered around 0 or 180°, indicating that fibers were preferentially spread along the *x-y* plane during self-assembling.

Discussion

The data presented in this report demonstrate applicability of the fiber-tracking algorithm developed for computation of collagen fiber orientation from confocal image sets. The software package based on our algorithm was evaluated by computer simulation and statistical analysis, and subsequently it was applied to the images of three-dimensional collagen matrices in order to extract the three-dimensional orientation data.

The three-dimensional images were collected with a confocal microscope (CLSM) operating in backscattered-light mode. Compared to wide-field and electron microscopy, confocal microscopy provides several advantages for the study of thick ECM samples. First, CLSM collects information from a well-defined optical section rather than from the whole depth of a specimen. Second, it optically sections the specimen to create z-series images, which can be used to reconstruct the three-dimensional structure (Sheppard & Shotton, 1997). Additionally, samples used with backscattered light–based CLSM require neither staining nor any other form of chemical processing. Therefore this approach avoids artifacts associated with common microscope preparatory techniques (Voytik-Harbin et al., 2001).

Currently available image-processing methods for exploring orientation of individual fibers require either skeletonization (Pourdeyhimi et al., 1996*a*, 1996*b*, 1997*a*, 1997*b*, 1999) or Hilditch thinning (Krucinska et al., 1997; Krucinska, 1999*a*, 1999*b*). These approaches have several drawbacks. The thinning procedures are very sensitive to small variations at boundaries or inside objects, which result in artifacts. In case of thick fibers, skeleton searching may be initiated in an inappropriate direction (Pourdeyhimi et al., 1996*b*). Other published algorithms use gradient edge operators to provide information about local orientation of each

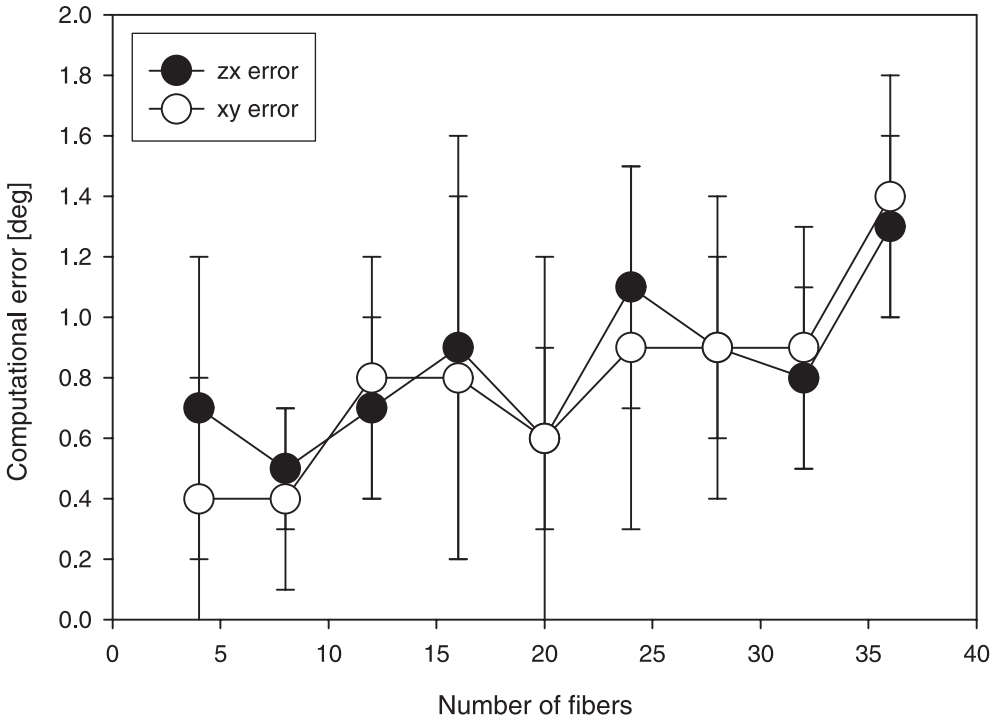

Figure 2. Accuracy of angle computations in three-dimensional space. Nine groups of data sets each with 10 image sets were created. Each image set consisted of 200 synthetic images (200 × 200 pixels). The number of randomly generated fibers in an image set ranges from 4 to 36. The orientations of generated fibers (real data) are compared to computed angles to measure the difference.

part of a fiber (Russ, 1999). If the fiber has many short side branches due to rough or irregular boundaries, the orientations of these branches contribute to the calculated distribution of fiber orientation, a likely source of error.

Unlike other published methods, our tracing procedure does not form fiber midlines by a series of connected pixels or voxels, but jumps from the center of one tracing element to another, forming a series of connected tracing elements along the midline. Both direction of searching and step size are critical in algorithms tracing fibrous structures. Our software used a circle (in two dimensions) or a cube (in three dimensions) to trace fibers. The size of the tracing element was determined by the tracing step size, which was automatically regulated on the basis of fiber thickness. Our approach reduces the tracking time and still obtains detailed structural information.

Some unwanted points not lying on midlines of fibers were often found in images of collagen matrices due to variations on the boundary of fibers. These points formed many short branches connected to the midline. Our algorithm was able to investigate their connecting mode and length and eventually truncate these artifactual branches. Thus, the identified midlines were accurate and robust with

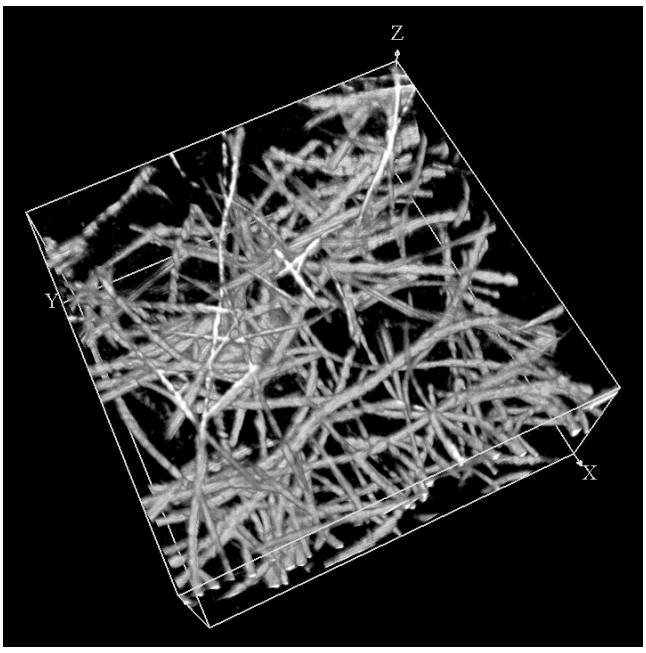

Figure 3. Volume-rendered three-dimensional reconstruction of a representative sample of collagen type I. Image size: 250 × 250 × 86 voxels, one voxel size: 0.254 μm × 0.254 μm × 0.6 μm. Sample was imaged with a confocal microscope operating in backscattered-light mode.

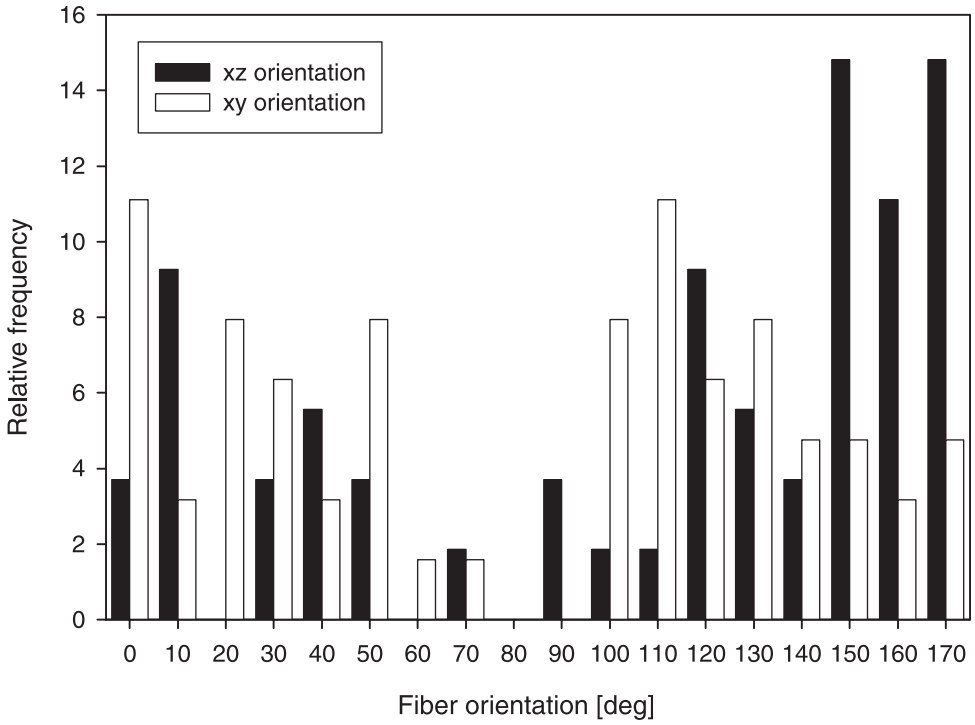

Figure 4. Orientation distribution of collagen fibers in a representative collagen sample. The three-dimensional fiber orientations projecting onto the *xy* plane and *xz* plane are labeled as *xy* orientation and *xz* orientation, respectively.

respect to variations in local fiber structure. Another advantage of our tracing program was that it could recover continuity of fibers that appeared to be discontinuous due to their reflecting properties. Based on their orientation and the size of gaps between them, our software could connect these segments to form a continuous fiber and thus provide a more accurate length and orientation information than previously possible.

Precise information about three-dimensional orientation of individual fibers is critical in investigating fiber formation, distribution, and interactions inside the collagen matrix. Integrating confocal microscopy with image-processing algorithms to derive three-dimensional quantitative data from the images of collagen matrix, we were able to show that fibers in collagen gels were arranged anisometrically. While distribution of *x-y* angles differed among tested samples, most collagen fibers spread along the *x-y* plane. Their *x-z* orientations were always close to 0 or 180°. Only a small number of fibers crossed the *x-y* planes, orienting themselves along the *z* axis. Since cell movement can be seriously influenced by collagen fiber orientation, these data provide important input in studies using collagenous matrices as a three-dimensional environment for cells (Dickinson et al., 1994; Friedl & Brocker, 2000; Gunzer et al., 2000).

Performed experiments and the current knowledge about collagen self-assembly do not allow us to speculate on forces that induce such a distribution of fibers during in vitro synthesis (Contard et al., 1993; Birk et al., 1995, 1997; Kadler et al., 1996; Brightman et al., 2000). More experiments are needed to explain the observed characteristics of collagenous networks; however, we believe that fiber-tracking techniques presented in this article may be applied to investigate this phenomenon.

Acknowledgments

Part of this research was supported by a Provost Reinvestment grant in Biological Imaging from Purdue University. B.R. was supported in part by a grant from the Polish Committee for Scientific Research (KBN 6PO4A07820).

References

Adams, C. & Fiona, M.W. (1993). Regulation of development and differentiation by the extracellular matrix. *Development* **117**, 1183–1198.

Aumailley, M. & Gayraud, B. (1998). Structure and biological activity of the extracellular matrix. *J Mol Med* **76**, 253–265.

Berthiaume, F., Moghe, P.V., Toner, M. & Yarmush, M.L. (1996). Effect of extracellular matrix topology on cell structure, function, and physiological responsiveness: Hepatocytes cultured in a sandwich configuration. *FASEB J* **10**, 1471–1484.

Birk, D.E., Nurminskaya, M.V. & Zycband, E.I. (1995). Collagen fibrillogenesis in situ: fibril segments undergo post-depositional modifications resulting in linear and lateral growth during matrix development. *Dev Dynam* **202**, 229–243.

Birk, D.E., Zycband, E.I., Woodruff, S., Winkelmann, D.A. & Trelstad, R.L. (1997). Collagen fibrillogenesis in situ: Fibril segments become long fibrils as the developing tendon matures. *Dev Dynam* **208**, 291–298.

Bissell, M.J., Hall, H.G. & Parry, G. (1982). How does the extracellular matrix direct gene expression? *J Theor Biol* **99**, 31–68.

Brightman, A.O., Rajwa, B.P., Sturgis, J.E., McCallister, M.E., Robinson, J.P. & Voytik-Harbin, S.L. (2000). Time-lapse confocal reflection microscopy of collagen fibrillogenesis and extracellular matrix assembly in vitro. *Biopolymers* **54**, 222–234.

Chen, C.S., Mrksich, M., Huang, S., Whitesides, G.M. & Ingber, D.E. (1997). Geometric control of cell life and death. *Science* **276**, 1425–1428.

Choquet, D., Felsenfeld, D.P. & Sheetz, M.P. (1997). Extracellular matrix rigidity causes strengthening of integrin-cytoskeleton linkages. *Cell* **88**, 39–48.

Contard, P., Jacobs, L., Perlish, J.S. & Fleischmajer, R. (1993). Collagen fibrillogenesis in a three-dimensional fibroblast cell culture system. *Cell Tissue Res* **273**, 571–575.

Curtis, A.S. & Wilkinson, C.D. (1998). Reactions of cells to topography. *J Biomat Sci—Polym E* **9**, 1313–1329.

Dickinson, R.B., Guido, S. & Tranquillo, R.T. (1994). Biased cell migration of fibroblasts exhibiting contact guidance in oriented collagen gels. *Ann Biomed Eng* **22**, 342–356.

Friedl, P. & Brocker, E.B. (2000). The biology of cell locomotion within three-dimensional extracellular matrix. *Cell Mol Life Sci* **57**, 41–64.

Gunzer, M., Friedl, P., Niggemann, B., Brocker, E.B., Kampgen, E. & Zanker, K.S. (2000). Migration of dendritic cells within 3-D collagen lattices is dependent on tissue origin, state of maturation, and matrix structure and is maintained by proinflammatory cytokines. *J Leukocyte Biol* **67**, 622–629.

Kadler, K.E., Holmes, D.F., Trotter, J.A. & Chapman, J.A. (1996). Collagen fibril formation. *Biochem J* **316**, 1–11.

Kleinman, H.K., Klebe, R.J. & Martin, G.R. (1981). Role of collagenous matrices in the adhesion and growth of cells. *J Cell Biol* **88**, 473–485.

Krucinska, I. (1999*a*). Evaluating fibrous architecture of nonwovens with computer-assisted microscopy. *Text Res J* **69**, 363–369.

Krucinska, I. (1999*b*). Evaluation of fibre orientation in fibrous materials. *Fibres Text East Eur* **7**, 45–50.

Krucinska, S., Krucinska, I., Veeravanallur, S. & Slot, K. (1997). Computer-assisted analysis of the extracellular matrix of connective tissue. *SPIE Proc* **3034**, 950–962.

Lo, C.M., Wang, H.B., Dembo, M. & Wang, Y.L. (2000). Cell movement is guided by the rigidity of the substrate. *Biophys J* **79**, 144–152.

Ottani, V., Raspanti, M. & Ruggeri, A. (2001). Collagen structure and functional implications. *Micron* **32**, 251–260.

Pelham, R.J., Jr. & Wang, Y.L. (1997). Cell locomotion and focal adhesions are regulated by substrate flexibility. *Proc Natl Acad Sci USA* **94**, 13661–13665.

Pourdeyhimi, B., Ramanathan, R. & Dent, R. (1996*a*). Measuring fiber orientation in nonwovens, part I: Simulation. *Text Res J* **66**, 713–722.

Pourdeyhimi, B., Ramanathan, R. & Dent, R. (1996*b*). Measuring fiber orientation in nonwovens, part II: Direct tracking. *Text Res J* **66**, 747–753.

Pourdeyhimi, B., Ramanathan, R. & Dent, R. (1997*a*). Measuring fiber orientation in nonwovens, part III: Fourier transform. *Text Res J* **67**, 143–151.

Pourdeyhimi, B., Ramanathan, R. & Dent, R. (1997*b*). Measuring fiber orientation in nonwovens, part IV: Flow field analysis. *Text Res J* **67**, 181–190.

Pourdeyhimi, B., Ramanathan, R. & Dent, R. (1999). Measuring fiber orientation in nonwovens, part V: Real webs. *Text Res J* **69**, 185–192.

Roeder, B.A., Kokini, K., Sturgis, J.E., Robinson, J.P. & Voytik-Harbin, S.L. (2002). Tensile mechanical properties of three-dimensional type I collagen extracellular matrices with varied macrostructure. *J Biomech Eng* **124**, 214–222.

Russ, J.C. (1999). *The Image Processing Handbook*. Boca Raton, FL: CRC Press.

Sheppard, C.J.R. & Shotton, D.M. (1997). *Confocal Laser Scanning Microscopy.* Oxford, UK: BIOS Scientific Publishers Ltd.

Stepien, E., Stanisz, J. & Korohoda, W. (1999). Contact guidance of chick embryo neurons on single scratches in glass and on underlying aligned human skin fibroblasts. *Cell Biol Int* **23**, 105–116.

Voytik-Harbin, S.L., Rajwa, B. & Robinson, J.P. (2001). Three-dimensional imaging of extracellular matrix and extracellular matrix-cell interactions. *Method Cell Biol* **63**, 583–597.

Wang, H.B., Dembo, M. & Wang, Y.L. (2000). Substrate flexibility regulates growth and apoptosis of normal but not transformed cells. *Am J Physiol—Cell Ph* **279**, C1345–C1350.

Wu, J. (2002). Ph.D. thesis. Three Dimensional Modeling of Engineered Extracellular Matrix Derived from Collagen. West Lafayette, IN: Purdue University.

Yamada, K.M. (1983). Cell surface interactions with extracellular materials. *Annu Rev Biochem* **52**, 761–799.